LANGMUIR

pubs.acs.org/Langmuir Article

Enhanced Thermal Conducting Behavior of Pressurized Graphene-Silver Flake Composites

Chiao-Xian Lin, Wei-Renn Tang, Li-Ting Tseng, Joey Andrew A. Valinton, Cheng-Han Tsai, Alfin Kurniawan, Kevin Chiou, and Chun-Hu Chen*

Cite This: *Langmuir* 2022, 38, 727−734 Read Online

ACCESS | Metrics & More | Article Recommendations | Supporting Information

ABSTRACT: Modern electronics continue to shrink down the sizes while becoming more and more powerful. To improve heat dissipation of electronics, fillers used in the semiconductor packaging process need to possess both high electrical and thermal conductivity. Graphene is known to improve thermal conductivity but suffers from van der Waals interactions and thus poor processibility. In this study, we wrapped silver microflakes with graphene sheets, which can enable intercoupling of phonon- and electron-based thermal transport, to improve the thermal conductivity. Using just 1.55 wt % graphene for wrapping can achieve a 2.64-times greater thermal diffusivity (equivalent to 254.196 ± 10.123 W/m·K) over pristine silver flakes. Graphene-wrapped silver flakes minimize the increase of electrical resistivity, which is one-order higher (1.4×10^{-3} Ω·cm) than the pristine flakes (5.7×10^{-4} Ω·cm). Trace contents of wrapped graphene (<1.55 wt %) were found to be enough to bridge the void between Ag flakes, and this enhances the thermal conductivity. Graphene loading at 3.76 wt % (beyond the threshold of 1.55 wt %) results in the significant graphene aggregation that decreases thermal diffusivity to as low as 16% of the pristine Ag filler. This work recognizes that suitable amounts of graphene wrapping can enhance heat dissipation, but too much graphene results in unwanted aggregation that hinders thermal conducting performance.

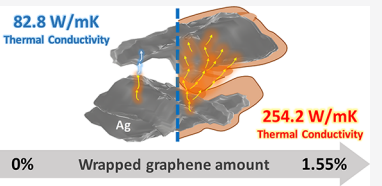

INTRODUCTION

With the rapid advances in the performance of electronic devices, one of the greatest challenges is inefficient heat dissipation.[1−4] Modern electrically conductive adhesives and/or pastes must effectively conduct heat and electricity to avoid heat accumulation. Silver flake fillers have been widely used as main conductive fillers to mix with organic resins for commercial conductive pastes,[5] where the elongated flake morphology is desirable to achieve high electrical conductivity. Because thermal transport in Ag dominantly relies on the electron transport mechanism,[6−8] any interruption on inter-particle contacts between Ag fillers can drastically decrease the heat conducting performance.[3,9,10] Phonon transport, on the other hand, delivers heat conduction through scattering and vibrations of lattice,[6,11] which should enable certain degrees of thermal conducting ability when an electron transport mechanism is not possible. Combination of Ag with phonon transport-dominant materials (e.g., graphene) is anticipated to increase the overall heat conducting performance for a wider range of applications whether contact and/or contact-free situations are involved; yet, this still requires confirmation.

Graphene exhibits a theoretical thermal conductivity as high as 5000 W/m K stemming from excellent phonon transport due to the unique 2D structures.[3,12,13] Several studies have incorporated graphene into adhesives as main or auxiliary fillers to improve the thermal conductivity.[14−16] For example, epoxy composites of the graphene-combined Cu, SiO_2, polystyrene, alumina, or boron nitride (BN) have been demonstrated to increase the thermal conductivity.[1,14,15,17−23] However, direct incorporation of graphene into resin or pastes is challenging. The large surface area of graphene drastically changes the viscoelastic properties of the pastes, resulting in processing difficulties. The strong $\pi-\pi$ attraction and van der Waals attraction between graphene sheets lead to severe local aggregation.[21,24,25] During processing, untreated graphene inevitably forms agglomerates that segregate in the polymer matrix. As such, designing interactions that prevent self-aggregation of graphene when combined with other conductive fillers could enable uniform graphene distribution in the new hybrid fillers and optimize thermal dissipation.

Previously, studies by Guo et al. have demonstrated the Ag-graphene heterojunction by direct decoration of Ag nanoparticles (~90 nm in diameter at average) onto graphene.[26] Because electron transport-assisted heat conduction of Ag requires sufficient volume to achieve, the nanoparticle form of Ag with much more quantized orbitals could not reach the same as that of the bulk Ag. Unlike the nanoparticle form, micrometer-sized Ag flakes have the appropriate sizes to provide suitable heat and electrical conductivities when

Received: October 3, 2021
Revised: December 17, 2021
Published: January 3, 2022

https://doi.org/10.1021/acs.langmuir.1c02631
Langmuir 2022, 38, 727−734

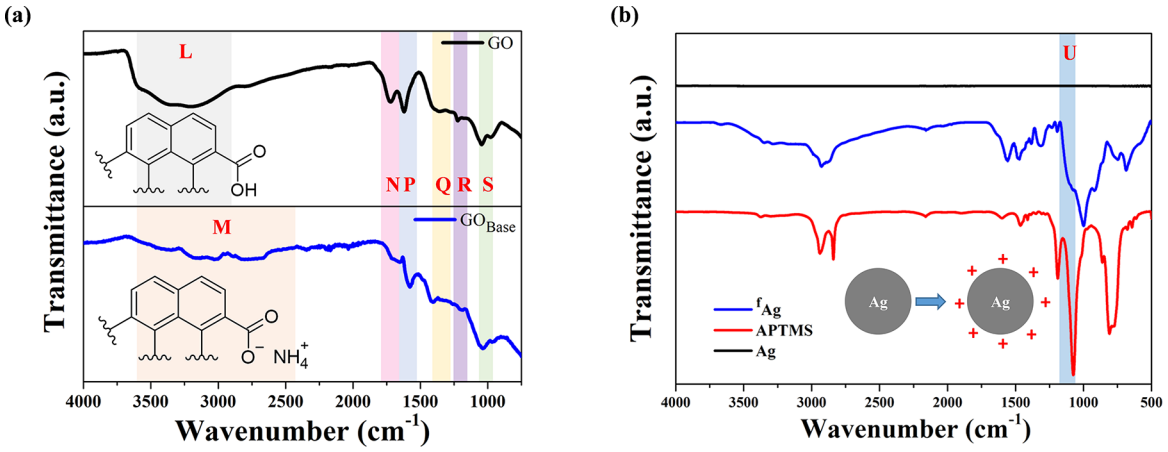

Figure 1. Characterization of modified graphene and Ag in the synthesized Ag-graphene composites. (a) IR spectra of GO (top) and GO_{Base} (bottom) show the protonated (inset, top) and deprotonated (inset, bottom) forms indicated by the changes in peaks from the O−H$^-$ band (L) to the N−H band (M); no change in peaks is seen in the other bands (N, P. Q, R, and S bands). (b) IR spectra of Ag and ^{f}Ag show the positively charged surface modification in Ag by APTMS (inset); the presence of Si−O−Si peaks at 1150 cm^{-1} (U) indicate the surface organosilane moieties attached.

combined with graphene. Nevertheless, examples of graphene-to-Ag microflakes used for studying thermal conductivity have not been carried out before.

In this work, we established an electrostatic attraction between graphene and silver where graphene sheets can wrap around the surface of micrometer scale Ag flakes. Such a strategy was intended to facilitate the formation of homogeneous Ag/graphene interfaces. We found that the compressed pellets of silver flakes wrapped with only 1.55 wt % graphene already exhibit an enhanced thermal diffusivity that is 2.64 times higher than that of pristine Ag flakes. Such an enhancement is mainly attributed to the inter-coupled electron−phonon transports and establishment of effective heat conduction channels.

EXPERIMENTAL SECTION

Materials. Graphite flakes (325 mesh, 99.8%; Acros), potassium permanganate ($KMnO_4$, ≥99%; J.T. Baker), 3-aminopropyltrimethoxysilane (APTMS, 97%; Alfa Aesar), silver microflakes (synthesized using surface stabilizers, particle size: 3−6 μm; Ample Electronic Co.), sulfuric acid (H_2SO_4, ≥96%; AENCORE), hydrogen peroxide (H_2O_2, 35%; Showa), hydrochloric acid (HCl, ≥37%; J.T. Baker), ammonium hydroxide (NH_4OH, 28%; Showa), and all solvents were purchased from commercial suppliers and used without further purification.

Synthesis of Base-Treated Graphene Oxide (GO). GO was synthesized in-house via the improved Hummer's method (the so-called preformed acidic oxidizing medium (PAOM) approach) reported in our previous work.[27] First, 3 g $KMnO_4$ was added to concentrated H_2SO_4 (23 mL) in an ice bath under stirring, followed by the slow addition of 1 g graphite powder and stirring for another 10 min. The whole mixture was then transferred to an oil bath at 35 °C under stirring for 12 h followed by an ice bath treatment for 10 min, where 50 mL deionized water was slowly added. After reheating at 85 °C for 15 min, the mixture was cooled in an ice bath for 30 min before 10 mL hydrogen peroxide was slowly added. The resulting GO product was filtered and successively washed with HCl and acetone. The base-treated GO solution was fabricated by reacting the GO aqueous dispersion (1 mg mL^{-1}) with ammonium hydroxide (28%, 3.5 mL) at 60 °C for 12 h followed by ultrasonication for 1 h (denoted as GO_{Base}).

Synthesis of Functionalized Silver Microflakes and Graphene-Wrapped Ag Composites. Surface functionalization of the obtained silver microflakes with the APTMS coupling agent was performed based on a previously reported method.[28−30] In a typical procedure, silver microflakes were uniformly dispersed in anhydrous toluene via sonication followed by the addition of APTMS (1 mM). After stirring overnight at room temperature, the functionalized silver microflakes (denoted as ^{f}Ag) were collected and thoroughly washed with ethanol to remove any unreacted APTMS and dried in an oven at 60 °C for 12 h. Functionalized Ag samples $^{0.1f}$Ag and $^{0.01f}$Ag were also made by using lower concentrations of APTMS (0.1 and 0.01 mM, respectively).

Graphene-wrapped Ag composites were prepared by mixing dispersions of pristine Ag or ^{f}Ag microflakes in ethanol (2 g, 200 mL) with GO (or GO_{Base}) aqueous dispersions (1 mg mL^{-1}, 20 mL) during 3 h of stirring. The GO suspensions required further sonication before use. The composite solids were then subjected to calcination at 350 °C for 2 h, which is enough to reduce the GO by deoxygenation (producing rGO), as described elsewhere.[38,39] The silver-to-rGO_{Base} mass ratio during synthesis was controlled at 100:1, 100:2, 100:3, 100:5, 100:10, and 100:15, denoted as Ag@rGO_{Base}-1, Ag@rGO_{Base}-2, Ag@rGO_{Base}-3, Ag@rGO_{Base}-5, Ag@rGO_{Base}-10, and Ag@rGO_{Base}-15, respectively. Afterward, the resultant solids were collected, thoroughly washed with water and ethanol, and dried in an oven at 60 °C for 12 h.

Materials Characterization. The morphology of the GO, GO_{Base}, and Ag@GO composite samples was examined with an FEI Inspect F50 field-emission scanning electron microscopy (FESEM) instrument operating at 5 kV. Fourier transform infrared (FTIR) spectra were recorded on a Perkin Elmer Spectrum Two spectrometer within the range of 4000−450 cm^{-1} at a 4 cm^{-1} spectral resolution. Confocal Raman measurements were performed on a WITec Alpha 300R microspectrometry instrument equipped with a frequency-doubled Nd:YAG laser emitting at 532 nm. In such a case, a Raman analysis is the only technique to verify the presence of graphene (neither X-ray or electron-based techniques can be useful). There is no intention to use Raman to determine the distribution or special functional group structures of graphene in the composites. All Raman spectra were collected at 10 randomly chosen locations within the 800−1800 cm^{-1} range with a 5 s integration time and then averaged. Thermogravimetric analysis (TGA) was carried out using a Perkin Elmer TGA 4000 instrument in the temperature range of 30 to 900 °C at a ramping rate of 10 °C min^{-1} in air. Elemental analysis was conducted with an Elementar Vario EL III CHNS/O analyzer. Differential scanning calorimetry (DSC) was measured with a Mettler Toledo DSC 1 in the temperature range of 30 to 400 °C at a ramping rate of 10 °C min^{-1} in air.

For cross-sectional SEM imaging and the thermal diffusivity measurements, the samples (1.2 g) were shaped into circular pellets

https://doi.org/10.1021/acs.langmuir.1c02631
Langmuir 2022, 38, 727−734

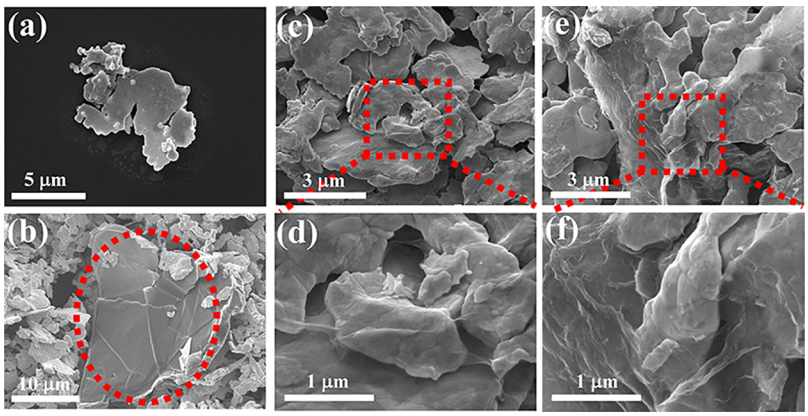

Figure 2. SEM images of the surface morphology of (a) the pristine Ag microflakes, (b) Ag@rGO, (c, d) Ag@rGO$_{Base}$, and (e, f) ^{f}Ag@rGO. The red-dashed ellipse in (b) shows graphene segregation from the Ag particles. The images in (d) and (f) are the magnified regions inside the red boxes in (c) and (e), respectively, showing graphene wrapping of Ag.

(12 mm in diameter and 1 mm in thickness) by applying a hydraulic pressure of 30 MPa. These pellet samples were placed inside a NETZSCH LFA467 HyperFlash at a Xenon flashlight voltage of 230 V, a duration of 396.57 ms, and a pulse width of 300 μs. The temperature of the measurements was kept at 30.0 ± 0.1 °C. To ensure effective flash absorption during the measurements, the surface of all samples was coated with a Kontakt Chemie Graphit 33 spray (CRC Industries, Belgium). In regard to the bulk resistivity measurements, copper was affixed to both sides of the pellets, which were then subjected to a digital multimeter. Tap density measurements were done using a Shin Kwang Machinery Tap-1 Tap Density Tester where around 5 cm^3 of the solid sample was placed on a 10 cm^3 glass cylinder and tapped for 2000 times at a rate of 220 taps per minute. The final tap density was calculated from dividing the mass by the final tapped volume.

RESULTS AND DISCUSSION

Establishment of the Interconnection between Graphene and Ag. To induce graphene wrapping around Ag flakes, electrostatic attraction by yielding negatively charged graphene (Figure 1a) or functionalizing Ag with positively charged APTMS (Figure 1b) was introduced.[28] In a typical experiment, highly oxidized GO was prepared according to prior publication.[27] GO was then deprotonated with ammonium hydroxide to generate negative charges (Figure S1).[31] According to the FTIR spectra of the graphene samples (Figure 1a), pristine GO (top) displays a strong and broad O−H stretching vibration (3000−3600 cm^{-1}, L), which is replaced by N−H stretching modes (2600−2950 cm^{-1}, M) in GO$_{Base}$ due to the attraction between negatively charged groups and protonated amine groups.[32] Ammonia treatment also causes a blue shift in the C═O stretching from 1720 to 1670 cm^{-1} (N) attributed to the electrostatic interaction between deprotonated carboxylic moieties and NH_4^+ ions, as supported by the elemental analysis where GO$_{Base}$ shows the presence of nitrogen (Figure S1b). Both spectra displayed aromatic C═C ring at (1621 cm^{-1}, P) vibrations, O−H deformation (1407 cm^{-1}, Q), C−OH stretching (1223 cm^{-1}, R), and epoxide C−O−C (900−1100 cm^{-1}, S).[33] To generate positive charges on the Ag flakes, we utilized the APTMS functionalization method.[27] In the corresponding FTIR spectra (Figure 1b), pristine Ag microflakes show no absorption at the 450−4000 cm^{-1} spectral region. ^{f}Ag distinctively shows Si−O−Si bending peaks (1150 cm^{-1}, U), which can be associated with linking of organosilane structures on the Ag surface.[34,35]

Figure 2 shows the morphological features of the as-synthesized composites. The pristine Ag flakes exhibit an irregular shape with a lateral dimension of 5−6 μm and a flat top surface (Figure 2a). Ethanol is a good dispersion solvent for both GO and Ag flakes but also capable of removing the surface stabilizing agents coated on the pristine Ag flakes. The presence of the surface stabilizing agent is identified using DSC (Figure S2a) and is characterized by the IR spectra (Figure S2b) as an unsaturated alcohol. This causes a slight deformation or aggregation of the relatively unestablished Ag surface toward rounding as seen in the SEM images (Figure S3). Such a phenomenon applies on all the Ag-graphene samples prepared using ethanol as the solvent.

For the samples prepared with the pristine Ag and GO (Figure 2b, denoted as Ag@rGO), the resultants exhibit no interconnection (i.e., by Coulombic forces) between the two components. The micrometer-sized GO pieces (marked with red-dashed lines) are segregated from the Ag particles with no observable graphene wrapping on the Ag surface (Figure 2b, red-dashed ellipse). Due to the functionalization of charges that promotes Coulombic interaction, Ag@rGO$_{Base}$ (Figure 2c,d) and ^{f}Ag@rGO (Figure 2e,f) possess notable graphene coverage on the Ag surface. The Raman spectra of Ag@rGO$_{Base}$ verified the presence of graphene, despite the small amounts (as low as 0.68 wt % by TGA, see below) and the lack of clear distinction in the SEM images (Figure S4). As such, interconnection based on the surface charges of either GO$_{Base}$ or ^{f}Ag is critical to achieve graphene wrapping without aggregation.

The amounts of wrapped graphene were investigated via TGA (Figure 3). The pristine silver flakes experienced no appreciable weight loss (<0.20%) up to 900 °C. For the negatively charged GO samples (Ag@rGO$_{Base}$-1), the weight loss is 0.68% at 900 °C, which is higher than that of Ag@rGO (0.52%) and pristine Ag (0.15%) at the same temperature. Ag@rGO$_{Base}$-5 and Ag@rGO$_{Base}$-10 show a trend of increasing weight loss (1.55 and 3.76%, respectively), which correlates well with the amount of graphene added, as shown in Figure S5. In terms of functionalizing Ag with positive surface charge, the ^{f}Ag@rGO samples exhibit an even higher weight loss of 3.30%. The huge mass loss in ^{f}Ag@rGO than Ag@rGO$_{Base}$ suggests that the positive functionality enabled higher degrees of graphene wrapping. As such, surface charge modification is

https://doi.org/10.1021/acs.langmuir.1c02631
Langmuir 2022, 38, 727−734

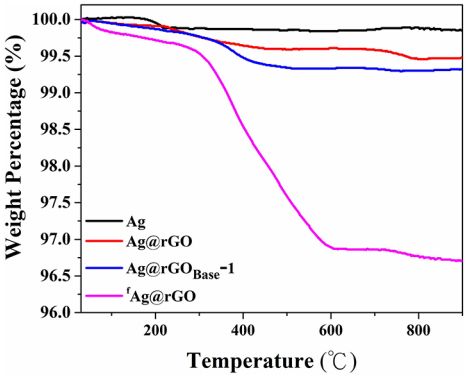

Figure 3. TGA curves of silver and the Ag-rGO composite samples recorded in air.

an effective strategy to manipulate the amounts of graphene attached onto the Ag surface.

Reduced GO is less conductive than Ag, so fully wrapping over Ag flakes lowers the overall electrical conductivity by forcing the electrons to go through the less conductive rGO.[36,37] Silver (with electrical resistivity of 10^{-5} Ω·cm),[38] like most metal conductors, relies on electron flow for the electrical and thermal conductivities as described by the Wiedemann–Franz law.[6] In the case of graphene, electron flow is limited in the two-dimensional plane resulting in a high bulk electrical resistivity (~10^{3} Ω·cm).[39] On the other hand, heat flow in graphene is dominated by phonon transport,[6] where scattering is possible across sheets,[6,11] resulting in an excellent bulk thermal conductivity (~10^{3} W/m·K)[12] higher than Ag (~10^{2} W/m·K).[40] Thus, the electrical conductivity of graphene-wrapped Ag should lie between the eight-order gap between Ag and graphene. The experimental results (Table 1) show

Table 1. Bulk Resistivity Values of Ag@GO$_{Base}$ Compared to those of the Pure Ag Samples

sample	Ag solid	Ag powder	Ag@ GO$_{Base}$-1	Ag@ GO$_{Base}$-5
bulk resistivity (×10^{-4} Ω·cm)	3.8	5.7	14	14

that the resistivity of the pristine silver flakes is 5.7 × 10^{-4} Ω·cm, slightly lower than that of Ag@rGO$_{Base}$-1 at 1.4 × 10^{-3} Ω·cm. This suggests that the homogeneously distributed, thin GO wrapping over the major surface of Ag flakes, despite the small amount of graphene in Ag@rGO$_{Base}$-1 (0.68 wt %), obstructed the electron path and slightly affected the bulk electrical conductivity. A reviewer suggested that aggregation and inhomogeneous distribution could reduce the effective cross section in the samples and also result in decreased electrical conduction. This scenario can be true, but only in cases with much higher graphene loading amounts (e.g., >10%, estimated). Aggregation of small quantities of GO cannot block electrical paths between the entire population of Ag particles and could not appreciably influence the bulk conductivity. As such, the obtained resistivity changes support the homogeneous distribution of graphene across the Ag surface.

Thermal Conducting Behavior. Effective thermal transport behavior in graphene-wrapped Ag composites can be highlighted through thermal diffusivity measurements.[41,42] Although thermal conductivity (κ) is the dominant indicator of thermal transport, thermal diffusivity (α) can be directly related to κ by the following equation:

$$\alpha = \frac{\kappa}{\rho \cdot C_P} \tag{1}$$

The direct relationship can be drawn on constant density (ρ) and heat capacity (C_P). In the case of Ag and graphene-wrapped Ag samples even with differences in graphene contents (Table 2), the observed similarities in density and heat capacity makes effective thermal transport to transitively equate to high thermal diffusivity. A summary of the thermal diffusivity of the graphene-wrapped Ag composites is shown in Figure 4.

The measured thermal diffusivity of the pristine Ag flakes is 43.8 $mm^2 \cdot s^{-1}$. Ag@rGO$_{Base}$-1 exhibits an enhancement in thermal diffusivity (52.0 $mm^2 \cdot s^{-1}$) over the pristine Ag flakes (43.8 $mm^2 \cdot s^{-1}$). The enhancement is further elevated in Ag@rGO$_{Base}$-5, with a 267% increase (115.8 $mm^2 \cdot s^{-1}$) over the pristine Ag. The control samples of physical mixing of the pristine Ag flakes and graphite or rGO (denoted as Ag + graphite or Ag + rGO, respectively, in Figure 4) exhibits the lower thermal diffusivity (36.8 and 27.4 $mm^2 \cdot s^{-1}$, respectively) than those of pristine Ag, suggesting that wrapping graphene around silver flakes is indeed critical to enhance the thermal conducting performance.

Meanwhile, ^{f}Ag exhibits that a significant decrease in thermal diffusivity of 2.8 $mm^2 \cdot s^{-1}$ as APTMS, even at miniscule amounts, forms grafted organosilanes that insulates heat[1,18]

Table 2. List of Thermal Conductivities and Diffusivities of Graphene-Wrapped Ag Samples in this Study in Comparison with Pure and Physically Mixed Samples

sample name	density (g/cm^3)	specific heat (J/g·K)	thermal diffusivity (mm^2/s)	thermal conductivity (W/m·K)
Ag	9.75 ± 0.22	0.19 ± 0.01	43.784 ± 1.751	82.809 ± 3.243
Ag + graphite	9.41 ± 0.22	0.22 ± 0.01	36.799 ± 1.472	76.181 ± 3.047
Ag + rGO	9.11 ± 0.21	0.19 ± 0.01	27.451 ± 1.098	47.994 ± 1.900
graphite	2.07 ± 0.05	0.77 ± 0.02	12.119 ± 0.485	19.229 ± 0.773
^{f}Ag	4.73 ± 0.11	0.55 ± 0.02	2.800 ± 0.112	7.272 ± 0.291
^{f}Ag@rGO	8.42 ± 0.19	0.25 ± 0.01	14.723 ± 0.589	30.737 ± 1.240
Ag@rGO$_{Base}$-1	9.50 ± 0.22	0.23 ± 0.01	52.028 ± 2.081	114.139 ± 4.547
Ag@rGO$_{Base}$-2	9.42 ± 0.21	0.22 ± 0.01	65.607 ± 2.624	138.451 ± 5.438
Ag@rGO$_{Base}$-3	9.71 ± 0.22	0.22 ± 0.01	73.665 ± 2.947	157.298 ± 6.295
Ag@rGO$_{Base}$-5	9.50 ± 0.21	0.23 ± 0.01	115.821 ± 4.633	254.196 ± 10.123
Ag@rGO$_{Base}$-10	9.28 ± 0.21	0.22 ± 0.01	6.912 ± 0.276	14.298 ± 0.563
Ag@rGO$_{Base}$-15	9.23 ± 0.21	0.22 ± 0.01	5.584 ± 0.223	11.292 ± 0.453

https://doi.org/10.1021/acs.langmuir.1c02631
Langmuir 2022, 38, 727−734

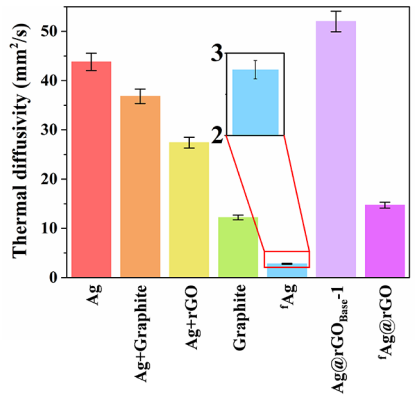

Figure 4. Comparison of the thermal diffusivity between the conductive fillers Ag@rGO$_{Base}$-1, ^{f}Ag@rGO, the pure samples (Ag, ^{f}Ag, and graphite), and physical mixtures (Ag + graphite and Ag + rGO). Inset magnifies the thermal diffusivity error bars in the ^{f}Ag sample.

[for details, see Supporting Information, Figure S6]. Nevertheless, ^{f}Ag@rGO still showed an increased thermal diffusivity from ^{f}Ag to 14.7 mm^2·s^{-1}, confirming the effectiveness of graphene wrapping through positively, despite in the presence of a thermal insulating layer.

Influence of the Graphene Loading Amount on the Thermal Conducting Property. The relation between thermal diffusivity and graphene loading amounts in the composite fillers was evaluated to further optimize the heat dissipation performance. As shown in Figure 5, Ag@rGO$_{Base}$-1

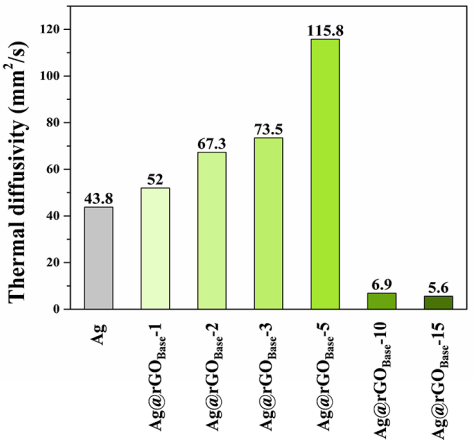

Figure 5. Bar diagram comparing the thermal diffusivity of the Ag@rGO$_{Base}$ composites at the various Ag:rGO mass ratios (100:1–100:15) as compared with the pure Ag sample.

and Ag@rGO$_{Base}$-5 (initial Ag:graphene ratios are 100:1 and 100:5) has a thermal diffusivity of 52.028 ± 2.081 mm^2/s and 115.821 ± 4.633 mm^2/s, respectively. Moreover, Ag@rGO$_{Base}$-2 and Ag@rGO$_{Base}$-3 (Ag:graphene at 100:2 and 100:3) has thermal diffusivities at 65.607 ± 2.624 mm^2/s and 73.665 ± 2.947 mm^2/s, respectively, providing a positive correlation between graphene loading and thermal diffusivity. However, the case of Ag@rGO$_{Base}$-10 (Ag:graphene = 100:10), with a TGA-based graphene content 2.42 times more than Ag@rGO$_{Base}$-5 (Figure S5), results in a plunge of thermal diffusivity at 6.912 ± 0.276 mm^2/s, retaining just ~5% of the value Ag@rGO$_{Base}$-5. This worsens with Ag@rGO$_{Base}$-15 (Ag:graphene = 100:15) with 5.584 ± 0.223 mm^2/s.

To understand the graphene loading effect, a series of cross-section studies was done on the composite fillers (from zero graphene content to Ag:graphene = 100:10) (Figure 6). The

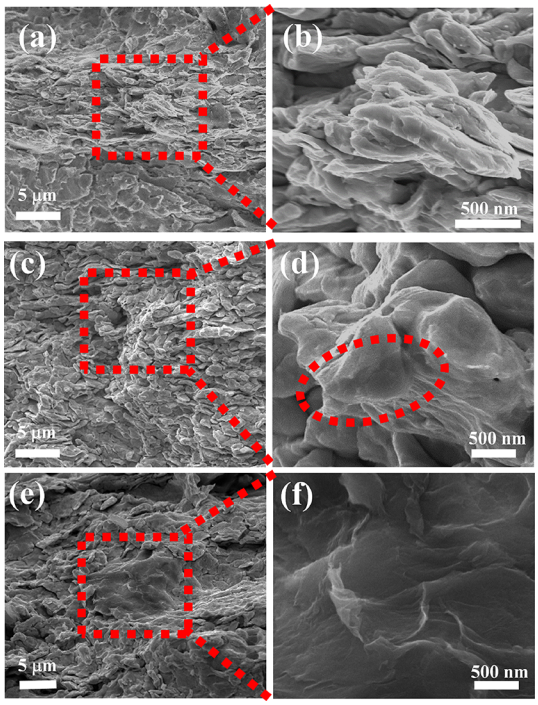

Figure 6. SEM cross-sectional images of the Ag@rGO$_{Base}$ ingot samples at the different Ag:rGO ratios. (a) Pure Ag sample with the magnified image (b) showing stacked Ag flakes; (c) Ag@rGO$_{Base}$-5 (Ag:rGO = 100:5) with the magnified image (d) showing the graphene coverage on Ag (marked with the red-dashed ellipse); (e) Ag@rGO$_{Base}$-10 (Ag:rGO = 100:10) showing extensive graphene agglomeration, as revealed in the magnified images (f) containing pure graphene. The red boxes in (c) and (e) show the origin of magnified images (d) and (f), respectively.

SEM images of the pristine Ag flakes show a stacking manner in the horizontal orientation, attributing to the response of the flake morphology to external pressure (Figure 6a,b). Ag@rGO$_{Base}$-1 shows negligible stacking behavior (Figure S7). In Ag@rGO$_{Base}$-5 (Figure 6c, d), only small amounts of wrapped graphene can be seen on the Ag flake surface. In Ag@rGO$_{Base}$-10 (Figure 6e,f), the SEM images show that there are sections of densely stacked rGO aggregates. Based on the thermal diffusivity data, these aggregates could be responsible for the degradation of the overall thermal diffusivity (Figure 6f).

Morphology Changes of the Graphene-Wrapped Ag Filler. With the issue of Ag deformation caused by ethanol, we conducted tap density measurement to evaluate degrees of morphology distortion in the graphene-wrapped Ag fillers. Multiple tapping ensures each particle to rearrange into its maximum space-filling capability as possible. For example, stacking of flake-shaped particles would have a high space-filling capability and thus a high tap density. Otherwise, the greater deformation on the flake morphology would lead to more stacking voids, which lowers the tap density values. In addition to SEM observation, tap density becomes a reliable bulk measurement to evaluate the morphological deformation degrees of the Ag flakes.

https://doi.org/10.1021/acs.langmuir.1c02631
Langmuir 2022, 38, 727–734

As shown in Figure 7, the tap density of the ethanol-treated silver flakes, denoted as Ag(ethanol), is 2.7 g·cm^{-3}, which is lower than the pristine ones (3.8 g·cm^{-3}), corresponding well to the DSC and SEM data (see Supporting Information) regarding the morphology deformation. In the case of graphene-wrapped Ag composites, their tap densities are 2.4 g·cm^{-3} (for Ag@rGO$_{Base}$-1) and 1.6 g·cm^{-3} (for Ag@rGO$_{Base}$-5) resulting to a 33% loss. As such, the data suggest the decreasing order of packing defects as follows: Ag@rGO$_{Base}$-5 > Ag@rGO$_{Base}$-1 > Ag(Ethanol) > Ag.

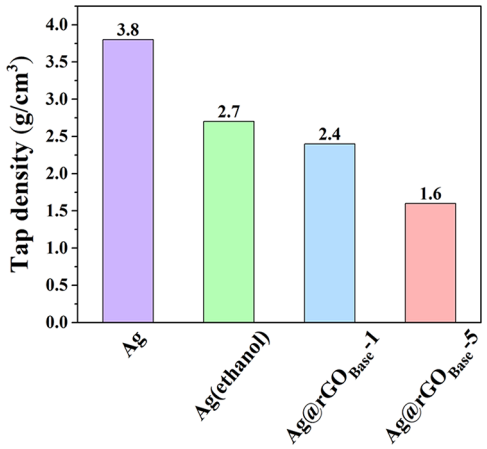

Figure 7. Bar graph comparing the tap density values of the synthesized fillers with Ag flakes in pure form and washed in ethanol [Ag(ethanol)].

Role of Graphene Wrapping in Thermal Diffusivity Enhancement. Our study highlights the direct influence of graphene on Ag interactions toward thermal diffusivity. With just the pristine Ag flakes compressed at 30 MPa without the presence of organics/resins, only resulting in a thermal diffusivity of 43.8 mm^2·s^{-1}, which is much lower compared to the ideal values (around 166 mm^2·s^{-1}) of a bulk Ag.[43] Such a difference is most likely due to packing defects created from the irregular stacking of Ag flakes after compression. According to the data, the addition of graphene introduced more irregular stacking (Figure 7). Yet, addition of graphene still improves thermal diffusivity. Our observations of uniform graphene coverage on the Ag flakes help us rationalize that the graphene sheets on the outer surface of the Ag flakes should bridge adjacent Ag flakes upon compression. As such, the graphene sheets connect every Ag flakes and establish pathways of heat conduction that lead to enhanced thermal diffusivity. Our results show that 1.55 wt % graphene content can optimally bridge the stacking voids due to the deformation of Ag flakes.

However, the samples with graphene contents greater than 1.55 wt % show lower thermal diffusivity (Figure 5) even compared to the physically mixed Ag-graphene samples (Figure 4). The significant drop of thermal diffusivity could be associated with the excessive stacking of graphene seen in the SEM images (Figure 6e,f). Although graphene has excellent thermal conductivity in the planar direction,[3,44,45] the out-of-plane thermal transport across the graphene stacks diminishes thermal conductivity.[46] Upon increasing layers of graphene (above 1.55 wt %), thermal transport eventually becomes weaker by phonon scattering across the graphene stacks.[47] This anisotropic behavior greatly reduces overall thermal diffusivity. This mechanism is illustrated in Scheme 1. Thus, an upper-limit on graphene sheets wrapping on Ag flakes should be established to prevent the presence of graphene stacks/agglomeration.

Scheme 1. Demonstration of the Heat Transfer Paths Created by Ag Flake Stacking Upon the Addition of Graphene[a]

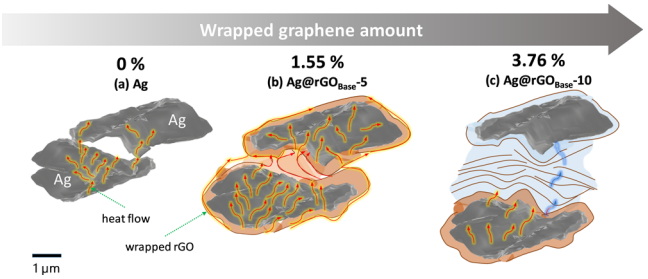

[a](a) The Ag flakes only transfers heat through direct Ag-Ag contact; (b) Ag@rGO$_{Base}$-5 shows that graphene provides optimal channels between Ag flakes for optimized heat conduction; and (c) Ag@rGO$_{Base}$-10 exhibits difficulty for heat transfer between Ag flakes due to excessive wrapping and aggregation.

Based on our resin-free study, we realized that enough amounts of graphene wrapping improve the heat flow within adjacent Ag particles. The effective heat transport on the composite cannot be realized through the addition of non-conductive resins nor thermal sintering. Meanwhile, extending this understanding toward the resin-based systems reported in the literature,[1,15,17] by comparison, requires the graphene loading amounts to be higher than this work (as a resin-free system) to achieve the optimal thermal conducting performance. This may suggest that the extensive network of graphene is needed to establish heat conduction across the non-conductive binder. As our resin-free system sets a limit of 1.55 wt % graphene to optimize heat diffusivity, Liu et al. demonstrated that a Cu@rGO core−shell filler with ∼4 wt % graphene content of resin-based pastes could improve the intrinsic thermal conductivity by 2.6 times.[1] Also, Chen et al. reported that loading of 12 wt % graphene on an organized alumina−graphene structure can achieve thermal conductivity enhancement by 19 times over the randomly blended counterpart.[15] This study, along with other related literature, agrees that considerable amounts of graphene should be added, which is beyond our suggested optimal concentrations, to acquire appreciable enhancement in thermal conductivity. The addition of resins spaces out the conductive microparticles, so these composites need more graphene nanosheets to establish an effective thermal conduction pathway. Overall, effective thermal diffusivity in resin-based paste systems may only be achieved once a percolation threshold is reached without overwrapping or aggregation of graphene.

CONCLUSIONS

In this study, we confirmed that graphene wrapping of Ag flakes, which enables intercoupling of phonon and electron transports, results in a higher thermal diffusivity than that obtained via physical mixing. Based on the graphene contents considered in this study, graphene nanosheets provide bridges connecting silver flakes to establish heat conducting channels to improve overall thermal diffusivity. For instance, the addition of graphene up to a Ag/graphene precursor mass

https://doi.org/10.1021/acs.langmuir.1c02631
Langmuir 2022, 38, 727−734

ratio of 100:5 (resulting in a 1.55% rGO content) can elevate the thermal diffusivity 2.64 times (i.e., from 43.8 $mm^2 \cdot s^{-1}$ for the pristine silver flakes to 115.8 $mm^2 \cdot s^{-1}$). To achieve highly thermally conductive ECAs, this research suggests that (1) local graphene agglomeration should be avoided; and (2) effective interconnections among conductive fillers via graphene, whether in the presence of non-conductive resin or not, should be established to allow effective heat conduction.

■ ASSOCIATED CONTENT

Supporting Information

The Supporting Information is available free of charge at https://pubs.acs.org/doi/10.1021/acs.langmuir.1c02631.

Elemental analysis of GO and GO_{Base}, Raman characterization data, Ag flakes stabilizing agent characterization (IR and DSC), SEM of Ag flakes before and after ethanol washing, TGA of Ag@rGO_{Base} at different Ag:GO ratios, thermal conductivities of ^{f}Ag samples, and cross-sectional SEM of Ag@rGO_{Base}-1 (PDF)

■ AUTHOR INFORMATION

Corresponding Author

Chun-Hu Chen − *Department of Chemistry, National Sun Yat-sen University, Kaohsiung 80424, Taiwan;* orcid.org/0000-0002-3512-6880; Phone: 886-7-525-2000; Email: chunhu.chen@mail.nsysu.edu.tw; Fax: 886-7-525-3908

Authors

Chiao-Xian Lin − *Department of Chemistry, National Sun Yat-sen University, Kaohsiung 80424, Taiwan*

Wei-Renn Tang − *Department of Chemistry, National Sun Yat-sen University, Kaohsiung 80424, Taiwan*

Li-Ting Tseng − *Department of Chemistry, National Sun Yat-sen University, Kaohsiung 80424, Taiwan; Ample Electronic Co., Kaohsiung City 831, Taiwan*

Joey Andrew A. Valinton − *Department of Chemistry, National Sun Yat-sen University, Kaohsiung 80424, Taiwan;* orcid.org/0000-0002-5244-3765

Cheng-Han Tsai − *Department of Chemistry, National Sun Yat-sen University, Kaohsiung 80424, Taiwan*

Alfin Kurniawan − *Department of Chemistry, National Sun Yat-sen University, Kaohsiung 80424, Taiwan;* orcid.org/0000-0003-2867-355X

Kevin Chiou − *Department of Materials and Optoelectronic Science, National Sun Yat-sen University, Kaohsiung 80424, Taiwan*

Complete contact information is available at: https://pubs.acs.org/10.1021/acs.langmuir.1c02631

Author Contributions

The manuscript was written through contributions of all authors. All authors have given approval to the final version of the manuscript.

Notes

The authors declare no competing financial interest.

■ ACKNOWLEDGMENTS

We acknowledge the financial support of the joint research program provided by Ample Electronic Technology Co., Ltd. and the Ministry of Science and Technology (MOST) of Taiwan (Project No. 108-2622-M-110-001-CC2).

■ REFERENCES

(1) Liu, S.; Zhao, B.; Jiang, L.; Zhu, Y.-W.; Fu, X.-Z.; Sun, R.; Xu, J.-B.; Wong, C.-P. Core−shell Cu@rGO hybrids filled in epoxy composites with high thermal conduction. *J. Mater. Chem. C* **2018**, *6*, 257−265.

(2) Kawagoe, Y.; Surblys, D.; Matsubara, H.; Kikugawa, G.; Ohara, T. Cross-Plane and In-Plane Heat Conductions in Layer-by-Layer Membrane: Molecular Dynamics Study. *Langmuir* **2020**, *36*, 6482−6493.

(3) Tseng, L.-T.; Jhang, R.-H.; Ho, J.-Q.; Chen, C.-H. Molecular Approach To Enhance Thermal Conductivity in Electrically Conductive Adhesives. *ACS Appl. Electron. Mater.* **2019**, *1*, 1890−1898.

(4) Yap, P.-L.; Tung, T.-T.; Kabiri, S.; Matulick, N.; Tran, D.-N.-H.; Losic, D. Polyamine-modified reduced graphene oxide: A new and cost-effective adsorbent for efficient removal of mercury in waters. *Sep. Purif. Technol.* **2020**, *238*, 116441.

(5) Kishi, H.; Saruwatari, T.; Mototsuka, T.; Tanaka, S.; Kakibe, T.; Matsuda, S. Synergistic effect of phase structures and in situ sintering of silver fillers on thermal conductivity of epoxy/polyethersulphone/silver filler composites. *Polymer* **2021**, *223*, 123726.

(6) Balandin, A.-A. Thermal properties of graphene and nanostructured carbon materials. *Nat. Mater.* **2011**, *10*, 569−581.

(7) Zhao, Y.; Fitzgerald, M.-L.; Tao, Y.; Pan, Z.; Sauti, G.; Xu, D.; Xu, Y.-Q.; Li, D. Electrical and Thermal Transport through Silver Nanowires and Their Contacts: Effects of Elastic Stiffening. *Nano Lett.* **2020**, *20*, 7389−7396.

(8) Jain, A.; McGaughey, A.-J.-H. Thermal transport by phonons and electrons in aluminum, silver, and gold from first principles. *Phys. Rev. B* **2016**, *93*, No. 081206.

(9) Zhou, J.; Li, Y.; Wu, Y.; Jia, B.; Zhu, L.; Jiang, Y.; Li, Z.; Wu, K. Tuned Local Surface Potential of Epoxy Resin Composites by Inorganic Core-Shell Microspheres: Key Roles of the Interface. *Langmuir* **2019**, *35*, 12053−12060.

(10) Aradhana, R.; Mohanty, S.; Nayak, S.-K. Novel electrically conductive epoxy/reduced graphite oxide/silica hollow microspheres adhesives with enhanced lap shear strength and thermal conductivity. *Compos Sci Technol* **2019**, *169*, 86−94.

(11) Singh, D.; Murthy, J.-Y.; Fisher, T.-S. Mechanism of thermal conductivity reduction in few-layer graphene. *J. Appl. Phys.* **2011**, *110*, No. 044317.

(12) Abeykoon, P.-G.; Ward, S.-P.; Chen, F.; Adamson, D.-H. Chromatographic Approach to Isolate Exfoliated Graphene. *Langmuir* **2021**, *37*, 9378−9384.

(13) Balandin, A.-A. Phononics of Graphene and Related Materials. *ACS Nano* **2020**, *14*, 5170−5178.

(14) Liu, Z.; Chen, Y.; Li, Y.; Dai, W.; Yan, Q.; Alam, F.-E.; Du, S.; Wang, Z.; Nishimura, K.; Jiang, N.; Lin, C.-T.; Yu, J. Graphene foam-embedded epoxy composites with significant thermal conductivity enhancement. *Nanoscale* **2019**, *11*, 17600−17606.

(15) Chen, Y.; Hou, X.; Liao, M.; Dai, W.; Wang, Z.; Yan, C.; Li, H.; Lin, C.-T.; Jiang, N.; Yu, J. Constructing a "pea-pod-like" alumina-graphene binary architecture for enhancing thermal conductivity of epoxy composite. *Chem. Eng. J.* **2020**, *381*, 122690.

(16) Liang, X.; Dai, F. Epoxy Nanocomposites with Reduced Graphene Oxide-Constructed Three-Dimensional Networks of Single Wall Carbon Nanotube for Enhanced Thermal Management Capability with Low Filler Loading. *ACS Appl. Mater. Interfaces* **2020**, *12*, 3051−3058.

(17) Huang, L.; Zhu, P.; Li, G.; Lu, D. D.; Sun, R.; Wong, C. Core−shell SiO_2@RGO hybrids for epoxy composites with low percolation threshold and enhanced thermo-mechanical properties. *J. Mater. Chem. A* **2014**, *2*, 18246−18255.

(18) Shahil, K.-M. F.; Balandin, A. A. Graphene-multilayer graphene nanocomposites as highly efficient thermal interface materials. *Nano Lett.* **2012**, *12*, 861−867.

(19) Liem, H.; Choy, H.-S. Superior thermal conductivity of polymer nanocomposites by using graphene and boron nitride as fillers. *Solid State Commun.* **2013**, *163*, 41−45.
(20) Fu, Y.-X.; He, Z.-X.; Mo, D.-C.; Lu, S.-S. Thermal conductivity enhancement of epoxy adhesive using graphene sheets as additives. *Int. J. Therm. Sci.* **2014**, *86*, 276−283.
(21) Huang, J.; Yang, W.; Zhu, J.; Fu, L.; Li, D.; Zhou, L. Silver nanoparticles decorated 3D reduced graphene oxides as hybrid filler for enhancing thermal conductivity of polystyrene composites. *Composites, Part A* **2019**, *123*, 79−85.
(22) Lei, L.; Shan, J.; Hu, J.; Liu, X.; Zhao, J.; Tong, Z. Co-curing effect of imidazole grafting graphene oxide synthesized by one-pot method to reinforce epoxy nanocomposites. *Compos. Sci. Technol.* **2016**, *128*, 161−168.
(23) Eksik, O.; Bartolucci, S.-F.; Gupta, T.; Fard, H.; Borca-Tasciuc, T.; Koratkar, N. A novel approach to enhance the thermal conductivity of epoxy nanocomposites using graphene core−shell additives. *Carbon* **2016**, *101*, 239−244.
(24) Kao, W.-Y.; Chen, W.-Q.; Chiu, Y.-H.; Ho, Y.-H.; Chen, C.-H. General Solvent-dependent Strategy toward Enhanced Oxygen Reduction Reaction in Graphene/Metal Oxide Nanohybrids: Effects of Nitrogen-containing Solvent. *Sci. Rep.* **2016**, *6*, 37174.
(25) Suter, J.-L.; Sinclair, R.-C.; Coveney, P.-V. Principles Governing Control of Aggregation and Dispersion of Graphene and Graphene Oxide in Polymer Melts. *Adv. Mater.* **2020**, *32*, No. e2003213.
(26) Guo, Y.; Yang, X.; Ruan, K.; Kong, J.; Dong, M.; Zhang, J.; Gu, J.; Guo, Z. Reduced Graphene Oxide Heterostructured Silver Nanoparticles Significantly Enhanced Thermal Conductivities in Hot-Pressed Electrospun Polyimide Nanocomposites. *ACS Appl. Mater. Interfaces* **2019**, *11*, 25465−25473.
(27) Chen, C.-H.; Hu, S.; Shih, J.-F.; Yang, C.-Y.; Luo, Y.-W.; Jhang, R.-H.; Chiang, C.-M.; Hung, Y.-J. Effective Synthesis of Highly Oxidized Graphene Oxide That Enables Wafer-scale Nanopatterning: Preformed Acidic Oxidizing Medium Approach. *Sci. Rep.* **2017**, *7*, 3908.
(28) Lan, W.-J.; Chen, C.-H. Hybridization of Graphene in 3D Complex Nanovoids: Synergistic Nanocomposites for Electrocatalytic Reduction of Hydrogen Peroxide. *Electrochim. Acta* **2015**, *180*, 1014−1022.
(29) Taghavi, F.; Gholizadeh, M.; Saljooghi, A.-S.; Ramezani, M. Cu(ii) immobilized on Fe_3O_4@APTMS-DFX nanoparticles: an efficient catalyst for the synthesis of 5-substituted 1H-tetrazoles with cytotoxic activity. *Medchemcomm* **2017**, *8*, 1953−1964.
(30) Nasiri, M.; Hassanzadeh Tabrizi, S.-A.; Hamzehalipour Almaki, J.; Nasiri, R.; Idris, A.; Dabagh, S. Synthesis, functionalization, characterization, and in vitro evaluation of robust pH-sensitive CFNs−PA−$CaCO_3$. *RSC Adv.* **2016**, *6*, 84217−84230.
(31) Ebajo, V.-D., Jr.; Santos, C.-R.-L.; Alea, G.-V.; Lin, Y.-A.; Chen, C.-H. Regenerable Acidity of Graphene Oxide in Promoting Multicomponent Organic Synthesis. *Sci. Rep.* **2019**, *9*, 15579.
(32) Shen, Z.; Feng, J. Highly Thermally Conductive Composite Films Based on Nanofibrillated Cellulose in Situ Coated with a Small Amount of Silver Nanoparticles. *ACS Appl. Mater. Interfaces* **2018**, *10*, 24193−24200.
(33) Li, D.; Huang, J.; Huang, L.; Tan, S.; Liu, T. High-Performance Three-Dimensional Aerogel Based on Hydrothermal Pomelo Peel and Reduced Graphene Oxide as an Efficient Adsorbent for Water/Oil Separation. *Langmuir* **2021**, *37*, 1521−1530.
(34) Cheng, W.; Marsac, R.; Hanna, K.; Boily, J.-F. Competitive Carboxylate-Silicate Binding at Iron Oxyhydroxide Surfaces. *Langmuir* **2021**, *37*, 13107−13115.
(35) Zarinwall, A.; Waniek, T.; Saadat, R.; Braun, U.; Sturm, H.; Garnweitner, G. Comprehensive Characterization of APTES Surface Modifications of Hydrous Boehmite Nanoparticles. *Langmuir* **2021**, *37*, 171−179.
(36) Scandurra, A.; Francesco Indelli, G.; Graziana Spartà, N.; Galliano, F.; Ravesi, S.; Pignataro, S. Low-temperature sintered conductive silver patterns obtained by inkjet printing for plastic electronics. *Surf. Interface Anal.* **2010**, *42*, 1163−1167.
(37) Du, J.; Zhao, L.; Zeng, Y.; Zhang, L.; Li, F.; Liu, P.; Liu, C. Comparison of electrical properties between multi-walled carbon nanotube and graphene nanosheet/high density polyethylene composites with a segregated network structure. *Carbon* **2011**, *49*, 1094−1100.
(38) Walker, S.-B.; Lewis, J.-A. Reactive silver inks for patterning high-conductivity features at mild temperatures. *J. Am. Chem. Soc.* **2012**, *134*, 1419−1421.
(39) Kong, B.-S.; Yoo, H.-W.; Jung, H.-T. Electrical conductivity of graphene films with a poly(allylamine hydrochloride) supporting layer. *Langmuir* **2009**, *25*, 11008−11013.
(40) Wang, X.; Guo, W.; Zhang, H.; Peng, P. Synthesis of Free-Standing Silver Foam via Oriented and Additive Nanojoining. *ACS Appl. Mater. Interfaces* **2021**, *13*, 38637−38646.
(41) Shancita, I.; Cagle, C.; Kalish, I.; Dubé, P.; Abraham, J.; Hammond, B.; Warzywoda, J.; Pantoya, M.-L. Tailoring Thermal Transport Properties by Inducing Surface Oxidation Reactions in Bulk Metal Composites. *ACS Appl. Mater. Interfaces* **2021**, *13*, 18358−18364.
(42) Zheng, W.; Huang, B.; Koh, Y.-K. Ultralow Thermal Conductivity and Thermal Diffusivity of Graphene/Metal Heterostructures through Scarcity of Low-Energy Modes in Graphene. *ACS Appl. Mater. Interfaces* **2020**, *12*, 9572−9579.
(43) Baehr, H.-D., Heat conduction and mass diffusion. In *Heat and Mass Transfer*, Springer Berlin Heidelberg: Berlin, Heidelberg, 2006; pp. 105−251.
(44) Balandin, A.-A.; Ghosh, S.; Bao, W.; Calizo, I.; Teweldebrhan, D.; Miao, F.; Lau, C.-N. Superior Thermal Conductivity of Single-Layer Graphene. *Nano Lett.* **2008**, *8*, 902−907.
(45) Chen, S.; Wu, Q.; Mishra, C.; Kang, J.; Zhang, H.; Cho, K.; Cai, W.; Balandin, A.-A.; Ruoff, R.-S. Thermal conductivity of isotopically modified graphene. *Nat. Mater.* **2012**, *11*, 203−207.
(46) Li, Q.; Guo, Y.; Li, W.; Qiu, S.; Zhu, C.; Wei, X.; Chen, M.; Liu, C.; Liao, S.; Gong, Y.; Mishra, A.-K.; Liu, L. Ultrahigh Thermal Conductivity of Assembled Aligned Multilayer Graphene/Epoxy Composite. *Chem. Mater.* **2014**, *26*, 4459−4465.
(47) Ghosh, S.; Bao, W.; Nika, D. L.; Subrina, S.; Pokatilov, E.-P.; Lau, C.-N.; Balandin, A.-A. Dimensional crossover of thermal transport in few-layer graphene. *Nat. Mater.* **2010**, *9*, 555−558.

https://doi.org/10.1021/acs.langmuir.1c02631
Langmuir 2022, 38, 727−734